ADVANCED MATERIALS TECHNOLOGIES
www.advmattechnol.de

Single-Step Deformation Processing of Ultrathin Lithium Foil and Strip

Debapriya P. Mohanty, James B. Mann, Vijayakumar Niranjan Payathuparambil, Sweta Baruah, Jessica K. Román-Kustas, Andrew B. Kustas, Tatsuya Sugihara, Kevin P. Trumble, and Srinivasan Chandrasekar*

Next-generation, high-efficiency energy storage and conversion systems require development of lithium metal batteries. But the high cost of production and constraints on thickness of lithium (anode) foils continue to limit adoption for integration into battery cell architectures. Here, a novel lithium anode manufacturing solution is demonstrated – single-step production of ultrathin gauge foil formats directly from solid ingot. Hybrid cutting-based deformation processes, involving large plastic strains and strain rates, produce foil to sub-10 μm thickness, with surface quality even superior to present Li anode processing routes. Energy analysis shows the single-stage processing is ≈50% more efficient than conventional processing by extrusion-rolling. Through in situ force measurements and high-speed imaging of the cutting it also characterize – for the first time – the flow stress of Li to strain rates of 800 sec^{-1}, revealing a power-law relationship. The results present a paradigm shift in manufacturing and integration of solid lithium anodes for energy applications.

1. Introduction

There is considerable interest in processing lithium metal into thin and ultrathin gauge strip/foil formats for energy storage applications, ranging from rechargeable single cell batteries to electric vehicle batteries (EVBs).[1–6] Development of high-energy density, rechargeable batteries requires solid lithium anodes with thickness 10 to 500 μm. A grand challenge for solid anodes is cost-effective production of ultrathin Li foil (<50 μm), with surface quality comparable, or superior, to conventional rolled metal strip.[4,6] The ultrathin Li formats could enable remarkable performance enhancement opportunities for rechargeable batteries. We demonstrate that this challenge can be met by cutting-based deformation processes that can directly produce lithium strip with thickness as small as 10 μm.

Current production of thin-gauge lithium foil ranges from conventional deformation processing by extrusion and rolling/calendering, to vapor deposition and electrochemical methods.[6–9] In the conventional deformation processing, a large ingot is converted into thin strip by extrusion followed by rolling. This is largely patterned on production of metal sheet/foil (e.g., Al, Ti, electrical steels) for structural and electrical applications.[10–12] With these alloys, the foil processing involves 20–30 stages of incremental deformation by rolling – several stages of hot rolling (>0.3 Tm) for large thickness reductions, followed by cold-rolling for properties and dimensional quality.[13–17] The rolling processes, while capable for large-volume production, are multi-step, inflexible and energy intensive, posing constraints to product design and performance. Importantly, rolled-strip cost increases near-exponentially with decreasing section size into foil range with almost all metals, Li being no exception.[6,18]

With lithium, because of its very low yield strength ($\sigma_y \approx 1$ to 2 MPa), the initial large reduction from ingot (e.g., 200 mm diameter) to strip of intermediate thickness (≈2.5 mm) can be accomplished by a single-stage extrusion process.[6,7,19] Such large shape changes by extrusion would be inconceivable with most metals, because the corresponding large forces required would impose severe constraints on tooling/equipment engineering.

D. P. Mohanty, V. N. Payathuparambil, S. Baruah, K. P. Trumble, S. Chandrasekar
Center for Materials Processing and Tribology
Purdue University
West Lafayette, IN 47906, USA
E-mail: dmohant@purdue.edu

J. B. Mann
M4 Sciences Corporation
Lafayette, IN 47901, USA

J. K. Román-Kustas, A. B. Kustas
Material
Physical and Chemical Sciences Center
Sandia National Laboratories
Albuquerque, NM 87123, USA

T. Sugihara
Department of Mechanical Engineering
Osaka University
Osaka 565-0871, Japan

The ORCID identification number(s) for the author(s) of this article can be found under https://doi.org/10.1002/admt.202301315

DOI: 10.1002/admt.202301315

The extruded strip is then rolled to final thickness, typically 100 to 500 μm. Mechanical rolling to even smaller thickness, e.g., <50 μm ultrathin foil, is very difficult, if not impossible, due to sticking of the Li foil to the roller surface, and propensity of the Li to crack and tear[6] Various details on the extrusion/rolling of Li are not clear, or even available, in the literature, such as whether the workpiece is pre-heated, and the number of rolling stages used. What is clear however is that processing of thin-gauge Li foil with thickness <100 μm is prohibitively expensive, based on costs quoted or estimated.[4,6,9] Furthermore, it may not even be consistently achievable.

Given this state-of-the-art of Li foil production, it is of interest to develop new alternative processing routes. In this study, we show, for the first time, that cutting-based deformation processes can be a viable route for low-cost production of Li strip in thin and ultrathin gauge formats, with thickness of 10 to 560 μm. Lithium strip, with very good (commercial) quality, is produced directly from ingot in a single step of deformation without pre-heating. We show how the process (shear) deformation field can be tailored to overcome the unique workability challenges that Li poses for strip processing; these largely arise from the exceptionally low strength (hardness ≈0.6 HV, $\sigma_y \approx 2$ MPa) and high ductility of the Li. The process specific energy is found to be much lower than for strip by conventional deformation processing. First-of-a-kind yield stress data for Li at high strain rates, of relevance for applications,[20–22] is also obtained from the cutting. Since the strip-processing is single-step, employing compact infrastructure, it can be done in a controlled atmosphere, and even implemented at point-of-use. Implications for prototype implementation of the processes for Li- foil manufacturing are discussed.

2. Results and Discussion

Cutting is a large-strain deformation process, wherein continuous strip (chip) of thickness t_c is produced by linear sliding of a hard tool against a workpiece with speed V_o (**Figure 1**; Figures S1 and S2, Supporting Information). In the present study, the chip – in foil or strip form – is the end-product. The cutting of metals is fundamentally different from the peeling (cutting) of polymers in that there is intensive shear (plastic) deformation occurring in the metal during the chip formation process across a narrow shear plane (Figure 1). This intense deformation causes the strip thickness at the exit of the shear plane t_c) to be much greater than the thickness of the material entering the shear plane (t_o). Other consequences of this deformation are significant roughening of the strip back (free) surface due to unconstrained deformation (free surface) and differential grain-level deformation (microstructure-related),[23–25] and the microstructure/properties of the strip being usually much different from that of the initial workpiece material due to the intense plastic straining.[26,27] The back-surface roughening, or rather its suppression, is a critical problem that has to be solved for achieving production of metal strip with good surface and dimensional quality. In contrast, with polymers, the mechanics of the cutting is analogous to elastic peeling of adhesive tape (or of wood veneer), with negligible change in the strip thickness during its formation (t_c being negligibly different from t_o) even with ductile polymers.[28–30] For this reason, and also because of a lack of a "grain structure" with polymers, the back surface of peeled polymer strips is usually quite smooth. We highlight these important differences between the cutting of metals and polymers, here, also as it is often erroneously assumed that polymer peeling and metal cutting are one and the same process.

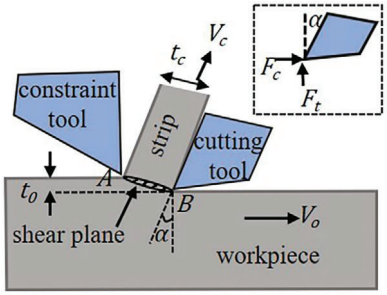

Figure 1. Schematic of Hybrid Cutting-Extrusion (HCE) process (plane strain) for Li strip. This shear-based deformation processing uses a constraint tool with the primary cutting tool to produce strip of pre-defined thickness (t_c). The controllable process parameters are workpiece speed V_o, tool rake angle (α) and undeformed chip thickness (t_0). Free Cutting (FC) is strip production without use of the constraint tool. AB is the deformation zone wherein strip formation occurs by large-strain shear deformation. The strain (ϵ) imposed in the strip is obtained from measurement of $\lambda = t_c/t_0$ and α, see Experimental Section. Inset shows cutting (F_c) and thrust (F_t) forces on the cutting tool.

We utilized two types of cutting methods to produce Li strip with thickness of 10 to 560 μm – 1) constrained cutting, called Hybrid Cutting Extrusion (HCE), wherein the strip is confined between the primary cutting tool and a constraint tool at the point of its formation (AB)[16,31,32] and 2) Free Cutting (FC),[24] wherein the strip is unconstrained. With both processes, we demonstrate that, by suitable design of the deformation zone geometry the strip back-surface roughening is fully or nearly-fully suppressed enabling production of Li strip with good surface and dimensional quality. The process parameters are shown in Figure 1, and **Table 1** lists the physical and mechanical characteristics/properties of the Li. Details about the mechanics of cutting and foil experiments are given in Experimental Section.

Table 1. Physical and mechanical characteristics of Li ingot and strip.

Li ingot	
Dimensions	50 mm diameter, 80 mm length
Recrystallization	≈0.5Tm (≈273K, ≈0 °C)
hardness (HV)	0.62 ± 0.03 kg mm^{-2}
σ_y	2.03 MPa
Li strip	
thickness (t_c)	10 to 560 μm
strain (ϵ)	≈1.35
hardness (HV)	0.70 ± 0.05 kg mm^{-2}
σ_y	2.3 MPa
Cutting specific energy	0.02 J mm^{-3} ≈ 0.040 MJ kg^{-1}

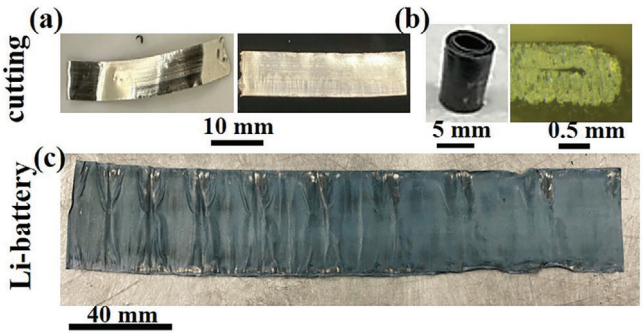

Figure 2. Lithium strip samples. a) Ultrathin gauge foil of thickness 25 μm (left) and thin-gauge foil of thickness 560 μm (right) produced by cutting. b) The cut Li foil of thickness 560 μm coiled to a 5 mm diameter roll (left) and, after a 180-degree bend, flattened onto itself (right) – 0T bend test – illustrating high formability/ductility. c) Li strip extracted from a commercial AA battery. The dark tarnish is due to exposure to the ambient atmosphere.

2.1. Strip Characteristics

Figure 2a shows optical microscope images of Li strip of width 10 mm, and two thicknesses, 25 μm (left) and 560 μm (right), produced by the cutting. The surfaces shown are the cut surface, viz., the strip surface in contact with the tool face (hereafter, cut surface; the opposite surface is the back surface). The cut surface is smooth and shiny except for minor striations near the lower edge, a consequence of tool cutting-edge roughness. See also Figure S3 (Supporting Information) for foils of other thickness. None of the strips showed any edge cracking. Edge cracking is usually common in rolled metal strip, often causing as much as 10% yield loss.[14,15,33] Each strip, including the thickest 560 μm one, could be wound tightly into a coil of diameter ≈5 mm as it was produced (tarnished in image). Also, the strip could withstand a 0T bend test[34] without cracking, attesting to its high ductility, see Figure 2b. For comparison, Figure 2c shows commercial Li foil of ≈300 μm thickness from an AA Li battery. Its surface resembles that of the strip produced by the cutting, except for the wrinkles which formed when the sample was uncoiled.

Figure 3 shows scanning electron microscopy (SEM) images of strip surfaces produced by the cutting. In the HCE (top row), the back surface is in contact with the constraint tool; while in the FC, this surface is unconstrained. Both cut and back surfaces of the HCE strip are quite smooth, also evident in the micrograph of the thickness x length cross section (top left). The smooth surfaces are a consequence of the large normal and shear stresses imposed by the tool and constraint. With the thicker 560 μm FC strip (2nd row), while the cut surface is smooth, the back surface shows some roughness due to unconstrained deformation of material occurring normal to the surface.[16,24,35] However, with the ultrathin 15 and 25 μm FC strips, both cut and back surfaces are smooth as with the HCE strip.

Surface topography measurements by optical profilometry (**Figure 4**, top), see Experimental Section, provided quantitative roughness information and confirmed the SEM inferences. It is seen from the figure (left column) that the S_a values (area roughness) on both surfaces of the HCE foil are quite small, and nearly identical, 1.42 μm (cut surface) versus 1.53 μm (back surface). The corresponding R_a values (line-scan roughness) are 0.39 and 0.41 μm. These R_a values are at the lower end of roughness commonly reported for commercial (rolled) metal strip (0.4 to 0.8 μm) such as Al and Cu.[14,36,37] With the ultrathin 15 and 25 μm FC foils, the R_a and S_a values on the cut and back surfaces are essentially the same as for the HCE strip indicating good surface quality. This reduction in the strip back-surface roughness in FC is enabled by the use of the tool with a large rake angle (35°) see also Experimental Section. However, with the thicker 560 μm FC strip, while the cut surface is smooth, the back surface roughness is greater, with S_a and $R_a \approx 10$X of that on the cut surface.

We explored the dependence of roughness on strip thickness (Figure 4 (bottom)). Interestingly, while the cut surface roughness is essentially independent of strip thickness, the back-surface roughness is seen to decrease (scale) with decreasing strip thickness into the ultrathin range. With the ultrathin 15 μm foil, the back surface and the cut surface have the same S_a and R_a; as also a 10 μm strip, the smallest thickness Li foil produced in the study. Foils produced from lead (Pb mimics deformation behavior of Li, see Experimental Section) also showed very similar roughness scaling with decreasing foil thickness down to 8 μm (see Figure S7, Supporting Information). These observations suggest that the cutting process is likely to be even superior to conventional extrusion/rolling in the ultrathin range.

The consistently small roughness observed on the cut surface, and the relative insensitivity of this roughness to cutting parameters, are a consequence of the large contact stresses imposed on this surface by the tool. Because of these stresses, the cut surface roughness is a replica of the tool surface topography, and negligibly influenced by process parameters.[16] This is also the case with the HCE-strip back surface which is smoothed by the deformation due to the high contact stress at the constraint. This smoothing by the constraint contact is the principal reason why the back-surfaces of HCE strips do not show much roughening. Interestingly, even with the 560 μm FC strip, when given a light cold rolling (CR) reduction of 20%, the S_a on the back surface reduced by 5X, to ≈3 μm, see Figures S4 and S5 (Supporting Information), and Refs.[14,16].

Since there is very little, large-area roughness data available for Li foil in the published literature (most of the data is AFM scans from micrometer-sized regions,[38] unsuitable for assessing roughness), we used commercial Li strip data as reference for additional comparative assessment. **Figure 5** shows SEM images of surfaces of the commercial Li strip. Figure S6 (Supporting Information) contains the profilometer images. Both surfaces of the commercial strip are smooth, with $S_a \approx$ 1.25 μm, like the HCE and ultrathin FC strips, confirming that the cutting processes can indeed produce commercial quality strip.

2.2. Mechanical Properties

The cutting imposes large strains in the strip during its formation. We characterized the strain (ϵ) using measurements of t_0 and t_c, and the strip hardness, see Experimental Section. Since the deformation process (Figure 1; Figure S2, Supporting Information) is essentially self-similar, ϵ depends only on the ratio $\lambda = t_c/t_0$. We selected a HCE condition of $\lambda = 2.5$, and strip thickness

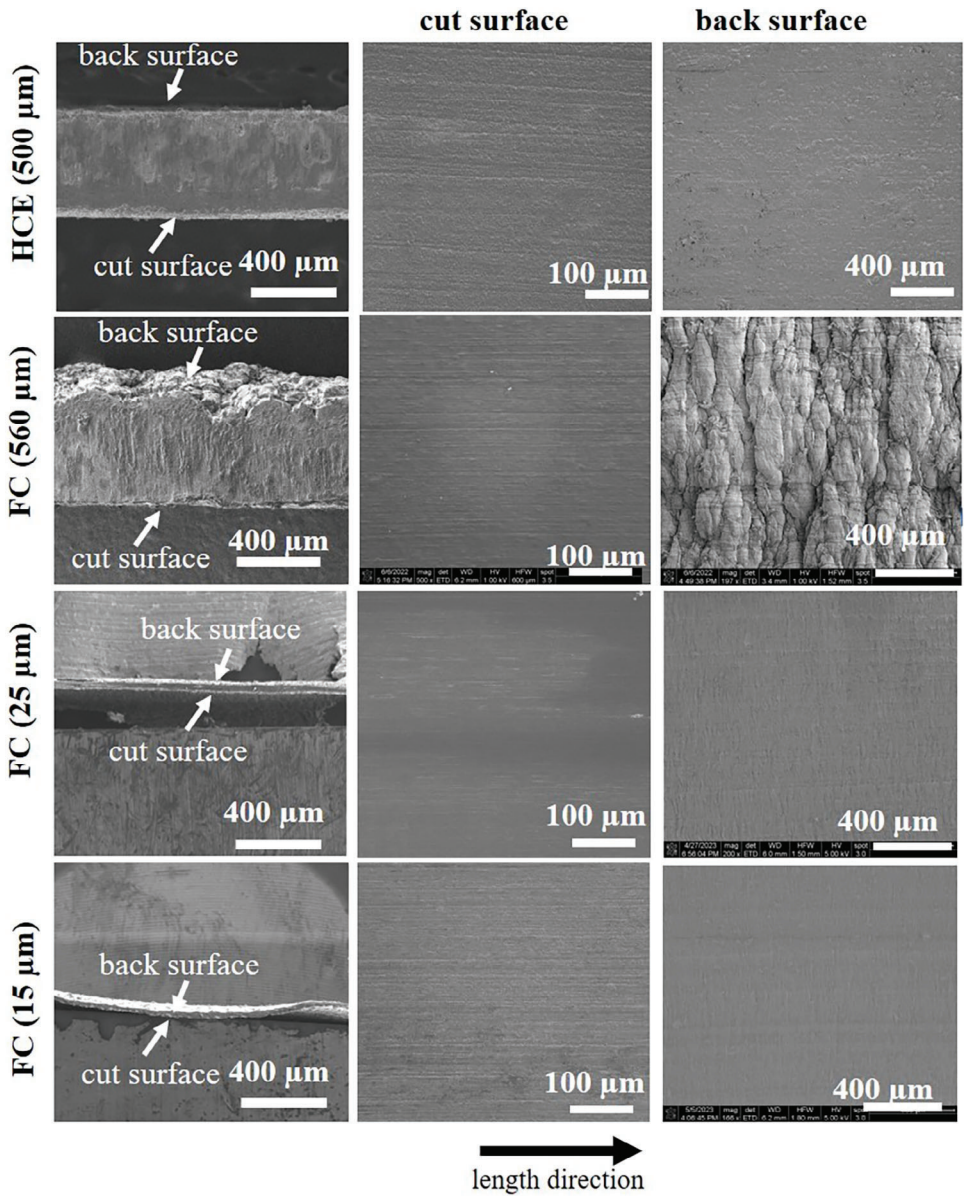

Figure 3. SEM images of strip surfaces (top) 500 μm strip, (2nd row) 560 μm strip, (3rd row) 25 μm strip, and (bottom) 15 μm strip. The left column images are of the thickness x length cross section, while the middle and right column images are of the cut and back surfaces, respectively.

of 500 μm, as this t_c is sufficiently large for accurate hardness measurement.

Table 1 gives the strain and hardness in the strip. The strip strain of 1.35 is large; for reference, this corresponds to a rolling thickness reduction of ≈75%. The strip hardness is 0.70 ± 0.05 HV, which is only marginally (≈13%) higher than the workpiece ingot (0.62 ± 0.03 HV). Assuming σ_y = HV/3 for metals,[39] we get the σ_y for the Li workpiece and strip as 2.03 and 2.3 MPa, respectively. The incremental change in the hardness (strength) during the HCE, despite the large ϵ, is very likely due to dynamic processes (recovery/recrystallization) occurring in the strip during cutting. These are to be expected since the ambient temperature of cutting (≈300 K) is well above the Li recrystallization temperature of ≈273 K (Table 1). Based on prior electron microscopy observations of Li foils produced by micro-cutting,[40] we anticipate our strips to be fine-grained, with grain size < 5 μm.

Insight into strip ductility, critical for applications, was obtained from the coiling and 0T bend tests (Figure 2b). First, the ability to coil the 560 μm thick strip into a tight circle of 5 mm diameter indicates that the strip is quite ductile. More definitive (quantitative) demonstration of high strip formability/ductility of is provided by the standard 0T bend test (Figure 2b).[34] At bend radius of "zero", where the strip is flattened onto itself, the maximum circumferential (bending) strain is ≈1. But no cracking was seen even in 5 repeat trials at this high tensile strain. This larger than expected ductility is likely due to crystallographic shear textures imposed in the strip by the cutting,[16,41,42] see Experimental Section and Figure S2 (Supporting Information).

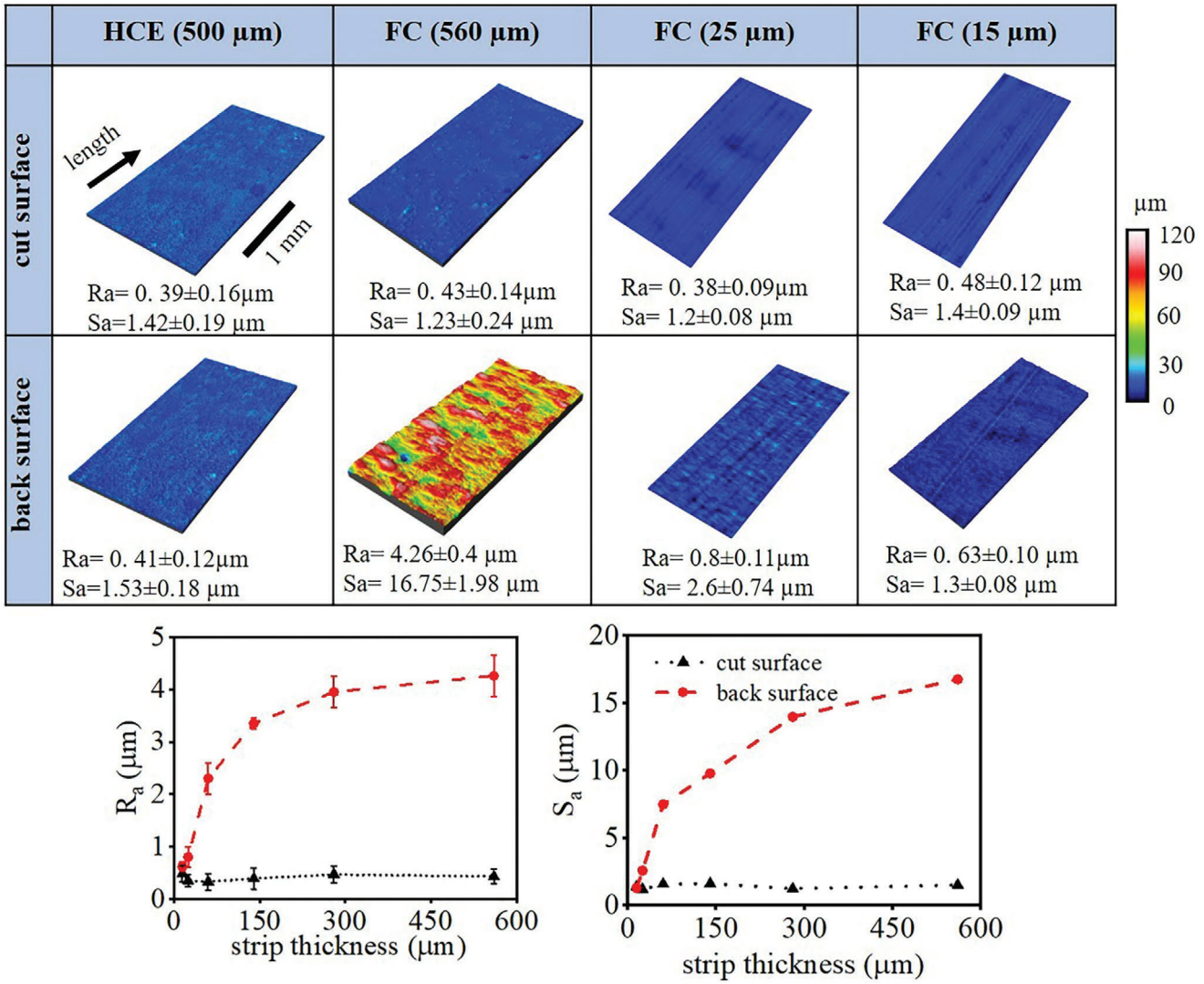

Figure 4. Surface topography of Li strips by optical profilometry. The top figure shows area profiles of the cut surface and back surface for various strips. The R_a and S_a are given in the images. Note the nearly identical surface roughness on both surfaces of the HCE strip. The line plots in the bottom figures show the variation of R_a and S_a with strip thickness for the two surfaces of strips produced by FC.

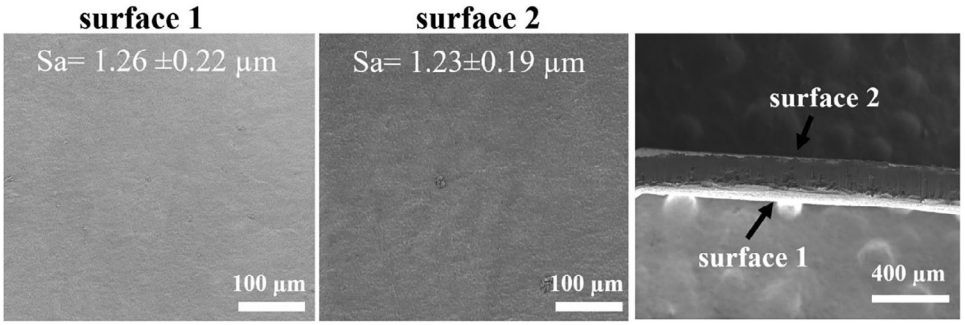

Figure 5. SEM images of commercial Li-foil surfaces. The left two frames are plan view images of the two principal surfaces, while the rightmost frame is a length x thickness cross section image.

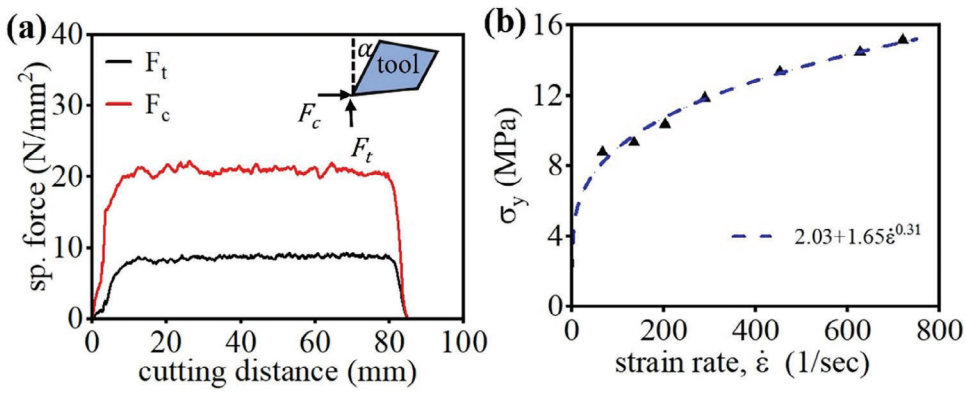

Figure 6. Strain rate dependence of flow stress (σ_y). a) Specific cutting (F_c) and thrust force (F_t) at V_o = 15 mm sec^{-1}. Inset shows orientations of F_c and F_t. b) Variation of σ_y with $\dot{\varepsilon}$. The trend line (curve) is a power law fit.

2.3. Yield Stress at High Strain Rates

The cutting experiments also helped measure the variation of Li yield (flow) stress with strain rate – data valuable for battery design, impact resilience, and life-cycle analysis. See Experimental Section for measurement details.

Figure 6a shows specific cutting (F_c) and thrust (F_t) forces in cutting of Li strip. This specific force is the measured force divided by the strip cross section area ($t_0 \times 10$ mm width). Figure 6b shows the variation of σ_y with $\dot{\varepsilon}$, derived from the forces and estimated strain rates. The strain in these experiments was constant at ≈1.35. A sharp increase in σ_y with $\dot{\varepsilon}$ is evident, with σ_y doubling from 8 to 16 MPa, when the strain rate changes from ≈50 to 800 sec^{-1}. If we include the quasi-static σ_y of ≈2 MPa (Table 1) from the hardness testing ($\dot{\varepsilon} \approx 0$) in the data, then the σ_y increase is 8-fold. The data is well-fitted by a power law, $\sigma_y = 2.03 + 1.65\dot{\varepsilon}^{0.31}$, as is typical for metals.

As noted earlier, the HCE strip hardness is only slightly different from the base workpiece, because of dynamic recovery/recrystallization during the cutting. However, Figure 6b shows that the operative (in situ) flow stress in the shear zone is much different — 5 to 8X that of the σ_y at low-strain rates (≈10^{-2} sec^{-1}) or in quasi-static testing (hardness test). This large increase in σ_y with $\dot{\varepsilon}$ is also consistent with the Li cutting being a hot-working process (≥0.5 Tm). Under such working conditions, the $\dot{\varepsilon}$ sensitivity of metals is known to be pronounced, especially for BCC metals like Li.[10,11] This high-strain rate data is first-of-a-kind. Prior tests have reported σ_y only to $\dot{\varepsilon} \approx 1$ sec^{-1}, using conventional mechanical testing.[43–45] The present approach also has the capability to measure σ_y at even higher strain rates (e.g., 10^4 sec^{-1}) by increasing V_o to ≈1 m sec^{-1}. Such strength characterization at large strains and high strain rates is not possible by conventional mechanical tests. The strain-rate data could be informative in the context also of safety design criteria for future battery systems in transportation applications, as high-rate deformation can occur in collisions.

2.4. Process Energy

It is of interest to compare the specific energy for strip production by the cutting-based methods with conventional deformation processing by multistage rolling/extrusion. This is done for two cases (500 μm strip thickness) – 1) conventional metal strip (Al6061-T6, 316 stainless steel (ss)) by multistage rolling, using data from industrial process schedules,[14,15] and 2) Li-strip by combined extrusion/rolling from initial ingot. See Experimental Section for details of the energy estimation.

For conventional metal strip (Al and 316ss), the principal conclusions were that the rolling energy is very large, ≈3.2 J mm^{-3} (1.190 MJ kg^{-1}) for Al, and ≈16 J mm^{-3} (2 MJ kg^{-1}) for 316ss; and ≈2/3 of this energy is for workpiece pre-heating (hot rolling stage) and the remaining 1/3 of energy is deformation energy.[14] The corresponding specific energy for Al strip by HCE was ≈0.72 J mm^{-3} (0.270 MJ kg^{-1}). The cutting energy is <30% of that of the rolling. Similar large energy reduction was also predicted for the 316ss. For Li strip by cutting, the specific energy was ≈0.02 J mm^{-3} (0.040 MJ kg^{-1}), using force data such as in Figure 6a. This energy is quite small compared to that for conventional metal strip, e.g., 0.72 J mm^{-3} for the HCE Al strip. The very small energy for Li is due to its "vanishingly" small σ_y. For the specific energy of Li strip by extrusion/rolling, we obtained a lower-bound value of ≈0.029 J mm^{-3}, also quite small. But even this lower bound is ≈50% larger than for the Li strip produced by cutting. The cutting-based processing thus offers attractive energy savings (>50%) for production of metal alloy strip.

3. Implications and Summary

We have shown that Li foil/strip, with thickness of 15 to 600 μm, and surface quality comparable, or superior, to commercial foil, can be produced by cutting processes. The keys to producing good surface finish in the Li strip are a) use of the constraint tool in the HCE that suppresses the strip back-surface roughening, often seen in free cutting (FC), by imposition of a high normal contact stress (compression), and b) use of a large rake angle ($\alpha > 25°$) tool in FC that intrinsically minimizes the deformation occurring in the direction normal to the strip free-surface conventional cutting of metals (this latter out-of-plane deformation is the main cause of the strip free-surface roughening). It is very difficult to produce ultrathin Li foil (e.g., <50 μm thickness) by conventional deformation processing, let alone cost-effectively. The cutting strip is created in a single deformation step, directly, from ingot, in contrast to the multistage extrusion and rolling. No

edge cracking was observed in any of the strips produced by the cutting. The strength of the HCE and FC foil is the same as that of commercial foil, thus meeting applications requirements also for mechanical properties. Besides demonstrating commercial-quality foil, the present study has also highlighted how cutting can be used to obtain flow stress of Li at high strain rates of ≈1000 sec^{-1}. A strong increase of σ_y with strain rate is seen, consistent with room-temperature deformation being hot-working for Li. Similar flow stress data at even higher strain rates of ≈10^4 sec^{-1} can be obtained by cutting tests at higher speeds (e.g., $V_o = 1$ m sec^{-1}).

It is useful to highlight the key attributes of the cutting-based processes for high-quality foil production and associated process conditions. First, the cutting can produce ultrathin foils quite readily in a single step from ingot. Second, the processes utilize compact equipment infrastructure and, consequently, can be configured to carry out foil production in a controlled atmosphere (e.g., glove box). In fact, the foil surfaces can also be protectively coated after the cutting by a suitable polymer film, as in rolling. The strip processing can be done at point of use, for example at battery assembly location, and integrated into roll-to-roll manufacturing systems. Thirdly, the process energy for the cutting is much lower than for conventional deformation processing. Fourthly, since the cutting is a single-step process, that utilizes commercially available tools, the foil processing cost could be much lower than by current methods.[6,46]

While we have demonstrated foil down to ≈10 μm thickness by the cutting-based routes, there is no fundamental barrier to using these processes to make Li foil of even near-zero thickness (e.g., 1 μm). With Pb, for example, we have already produced foils with thickness < 10 μm, see Figure S7 (Supporting Information). The main requirement for ultrathin foil manufacturing is availability of tools with sharp cutting-edge radius (<2 μm). Such a sharp edge can be a problem when cutting higher strength alloys; however, this is not a limitation with the very soft Li.

Similarly, scaling of the cutting to produce strip of larger width, with dimensions similar to commercial anodes, should be straightforward, by using a tool with a wider cutting edge (edge-width equal to or slightly greater than the strip width). The mechanics of the cutting process remains the same with wider cutting edges; the only change is in the cutting force/power which scales linearly with the strip width (more precisely with the strip cross section area). In fact, we have produced metal strips with width 50 to 100 mm (similar to anode or greater than anode dimensions in commercial AA batteries) from much higher-strength alloys like Cu 101, Al6061-T6, and electrical steels.[14,16] These alloys are 150 to 500 times harder than the Li of the present work. Length scaling is also feasible; for example, by using a rotary cutting configuration and a cylindrical workpiece, we have produced Al, Cu and Fe-Si alloy strip with length > 1000 mm. Examples of large-scale strip from the higher-strength alloys, that illustrate the length and width scaling achieved with HCE and FC on our current lab-scale cutting equipment, are provided in Figure S8 (Supporting Information).

Recently, we have used the rotary cutting configuration to produce Li strip of longer length, albeit with 1 cm width. The initial results are quite promising, see last frame of Figure S8 (Supporting Information) which shows the strip in situ on the machine after it has emerged from the process zone. Besides developing this rotary configuration for Li strip of longer lengths, we also plan to address the width scaling which has been currently hampered by lack of availability of Li billet/block (workpiece material) of sufficiently large size.

Other process requirements for foil production are a) a large-positive rake angle tool ($\alpha > 25°$), such as used here, to ensure smooth material flow and minimize the extent of surface roughening on the strip back surface in FC; b) a well-prepared, sharp tool edge, devoid of scratches, to ensure smooth foil surfaces; and c) tool coatings (e.g., diamond) that will minimize Li adhesion. With implementation of some of these changes to the process, we anticipate production of Li foil with thickness of 1 to 5 μm. It is useful to note that we could produce good quality foil, even with high-speed steel tools crafted in our laboratory to the above geometric specifications, in this proof-of-concept study.

Ongoing work is focused on extending the proof-of-concept of the cutting to produce foils with near-zero thickness; scaling up of the processing for larger foil widths (e.g., 50 mm); process systems design for integrating controlled ambient environments suitable for Li; metallurgical characterization of foil microstructure and texture; and comparative foil production-cost analysis paralleling the energy modeling.

4. Experimental Section

Li Strip Processing by Cutting–Mechanics and Process Configuration: Cutting is a large-strain deformation process, wherein a continuous chip (strip) of thickness t_c is produced by the sliding of a hard tool against a workpiece (Figure 1) with speed V_o. In the present study, the peeled chip – in foil or strip form – was the process end-product. This contrasts with conventional machining applications, where the cutting process was largely used to create component (workpiece) surfaces, and the chip is a "waste" product. Besides V_o, the key process parameters were the tool rake angle (α) and the undeformed chip thickness (t_0), see Figure 1 and Figure S1 (Supporting Information). The strip production (forming) occurs by intense shear confined to a narrow region, the shear zone AB. Conventional cutting, i.e., without the constraint in Figure 1,is referred to as Free Cutting (FC), here, to emphasize that the strip thickness at the shear zone exit (t_c) was not set a priori in this process but was a consequence (output) of the deformation. Typically, t_c was greater than t_0, in FC, because of the strip undergoing unconstrained deformation in zone AB during its formation.

The chip formation was converted into a strip-forming process – Hybrid Cutting Extrusion (HCE), with t_c set (controlled) a priori – by using a second constraint tool located directly across from the primary tool, see Figure 1.[16,31,32] In HCE, t_c could be set smaller or larger than t_0. Under conditions of plane strain, and uniform deformation, as in the present study, the von Mises strain (ϵ) imposed in the strip in zone AB could be well-approximated by Equation 1 (where $\lambda = t_c / t_0$[16,31]):

$$\varepsilon = \frac{1}{\sqrt{3}} \left(\frac{\lambda}{\cos(\alpha)} + \frac{1}{\lambda \cos(\alpha)} - 2\tan(\alpha) \right) \quad (1)$$

The strain rate in the deformation zone, another key attribute of the deformation field is, to first order, given by:

$$\frac{d\varepsilon}{dt} = CV_o\varepsilon \quad (2)$$

where C is a pre-determined constant that depends on the characteristic shear zone width. The strain rate varies essentially linearly with V_o.

Equations 1 and 2, taken together, provide an analytical characterization of the deformation field (strain and strain rate) in the shear zone AB in

terms of the (controllable) process parameters, λ, α and V_o. They also describe how the deformation in the HCE and FC could be varied/controlled. Plastic strains in the range of 0.5 to 10 and strain rates of 10 to 10^5 sec^{-1} could be imposed by selection of the process parameters.[47] It was these deformation parameters that determine the microstructure and properties of the strip material.

Other HCE and FC deformation zone attributes, complementing the intense/localized strain, were large hydrostatic pressure and adiabatic deformation heating.[31] This combination of deformation conditions was favorable for suppression of cracking and flow instabilities in the shear zone – an outstanding feature of this type of processing for Li strip production. In prior work, these favorable deformation field attributes were utilized to demonstrate single-step production of strip, from alloys as diverse as Al, Cu, high-Si electrical steels and Ti, for electrical and structural applications.[16] The strip products in these studies ranged from 5 to 100 mm in width, and 0.05 to 1 mm in thickness.

The proof-of-concept Li strip production experiments were done in a linear plane-strain cutting configuration analogous to Figure 1. Commercially pure Li ingot (>98% purity, United Nuclear, USA), 50 mm in diameter and 80 mm in length, was used as the workpiece. Table 1 gives the important physical and mechanical characteristics of the workpiece material and the strips. The cutting was done along an axial slot of depth 10 mm and width 10 mm that was machined within the ingot. The sides of the slot provided a natural constraint for plane strain deformation. An up-sharp high-speed steel (HSS) tool, with cutting edge width > 10 mm, rake angle $\alpha = 35°$ and edge radius (≈5 μm) was used. This rake angle was selected, based on screening experiments, as it ensured uniform (laminar) material flow through the shear zone and minimal strip back-surface roughening in FC, both critical for the strip processing. The very soft nature of the Li allows the use of rake angles as high as 45°. Similarly, the small tool edge radius enabled strip with thickness down to 15 μm to be repeatably produced. Strips of different thickness were produced, by varying t_0 and t_c, at V_o = 15mm sec^{-1}, see Figure 3. For the HCE, a constraint tool, also HSS, was added as in Figure 1.

The cutting process zone was submerged in a pool of mineral oil to minimize exposure of the Li strip to the ambient (lab) atmosphere. However, as the strip emerged from this zone, it was exposed to the lab ambient environment, resulting in the surfaces being tarnished (see, for example, the darker outer surface of the coil in Figure 2b). Since the present study was primarily concerned with demonstrating proof-of-concept, no attempt was made to carry out the experiments in a controlled ambient atmosphere.

The strips were collected and their dimensions (length, thickness t_c) were measured. After the measurements, the strips were packaged in a glass box under mineral oil and stored for further characterization (e.g., surface roughness, hardness). The thickness measurements also enabled estimation of λ and the strain imposed in the strip (Equation 1). For the experiments in the present study, λ was in the range of 2.5 to 3.

The cutting (F_c) and thrust (F_t) components of the deformation force, see Figure 1, were measured using a piezoelectric force dynamometer (Kistler 9254, natural frequency ≈2 kHz) coupled to the cutting system. The vector sum of these force components gives the resultant force. The forces were used to obtain flow-stress data for Li as a function of strain rate, and to estimate the process specific energy for Li strip production.

Material Flow and Deformation Analysis: High-speed in situ imaging of material flow in the deformation zone AB, coupled with digital image correlation (DIC) analysis, was used to characterize material flow and the deformation field in cutting. The objectives of this characterization were to identify process conditions that result in smooth laminar (uniform) flow of material in strip formation, ideal for achieving high-quality strip; establish the "sharpness" or width of the shear zone in cutting for flow stress (σ_y) estimation at various strain rates; and obtain the dependence of deformation-zone strain rate on V_o.

Figure S1 (Supporting Information) shows a schematic of the experimental arrangement used for the in situ high-speed imaging of material flow in cutting (FC and HCE). A high-speed camera (Photron Fastcam Mini), coupled to an optical microscope assembly, was used for the imaging. The spatial resolution of the imaging system was ≈1.4 μm per pixel. Framing rates of up to 2000 frames per second, sufficient for accurate flow field mapping, were used. Plane strain deformation conditions in the process deformation zone were ensured by constraining one side of the workpiece (imaging side) by a glass plate that was clamped against the workpiece length. The HCE and FC experiments were done at V_o of 2 to 100 mm sec^{-1}, in order to access a range of strain rates. More details about the high-speed imaging and image analysis can be found in Refs.[35].

The experiments to establish the deformation zone attributes were done with lead as a model material. The deformation characteristics of Pb mimic those of Li. Like Li, Pb is soft and ductile, and has a recrystallization temperature (0.5 Tm = 300 K) that is essentially room temperature (Note: The imaging could not be done directly in cutting of Li, since the workpiece in this case was typically flooded with mineral oil). To establish the confinement of flow in the shear zone, that was the "sharpness" of the shear zone, digital image correlation (DIC) analysis of the high-speed image sequences was used and mapped the strain rate field.[35] The strain rate field, the incremental strain imposed per unit time, demarcates the shear (deformation) zone. From this analysis, the deformation zone width could also be estimated.

Figure S1 (Supporting Information) (right) shows a time-averaged picture of the material flow in HCE, based on 200 consecutive frames from a high-speed image sequence. A sharp shear zone was seen, demarcating the boundary between the bulk workpiece and the strip (chip). This shear zone was even better demarcated in the strain rate fields (background color) shown in Figure S2 (Supporting Information), which were constructed from DIC analysis of image sequences of the material flow. The region of intense strain rate (≈70 sec^{-1}) demarcates the shear zone. The field details were shown for two values of λ. It was clear from the figures that the deformation was highly confined – the region of intense strain rate was of small width (≈40 μm) in the direction of strip flow – that it could be idealized as a shear plane; and the strain rates in the shear zone are quite high, 50 to 150 sec^{-1}. The average strain rate varied linearly with V_o, consistent with Equation 2, see also.[47]

Based on this shear plane idealization of the deformation, the yield stress (flow stress σ_y) of Li could be obtained as a function of strain rate from cutting (FC) experiments carried out at different V_o. This calculation involved estimation of $d\epsilon/dt$ in the shear zone AB at various V_o using Equation 2, and the assumption that plastic deformation occurs on the shear plane at a constant shear stress (shear yield stress τ).[47] The shear stress τ on the shear plane could then be estimated by resolving the measured resultant force (vector sum of F_c and F_t in Figure 1) along the shear plane, that was estimating the shear force F_s on the shear plane; and calculating τ as equal to F_s/A_s, where A_s was shear plane area. This τ, which represents a shear yield stress, could be converted to a uniaxial yield stress (σ_y) by using the von Mises relation for plane-strain deformation, $\sigma_y = \tau/\sqrt{3}$.

The flow stress estimation was done by using force data obtained at different strain rates (by varying V_o). Using measurements of t_c and t_0, in conjunction with Equations 1 and 2, the strain and strain rate in the shear zone were estimated for each V_o condition. The corresponding values of F_s, τ and σ_y were calculated as discussed above. By combining the two sets of data, the variation of σ_y with $\dot{\epsilon}$ was obtained, see Figure 6b. The strain in the strip over the range of strain rate conditions studied was constant, ≈1.35. The flow stress estimation could be done at even higher strain rates, e.g., 10^4 sec^{-1}, than those accessed in this study, by increasing V_o to 1m sec^{-1} and more.[47] This type of high strain-rate, material property data was difficult, if not impossible, to obtain using conventional mechanical testing.

The shear plane orientation, which controls the crystallographic texture in the strip, was strongly influenced by λ (see Figure S2, Supporting Information). The shear zone characteristics suggest that the strip will have a strong crystallographic shear texture, favorable for strip formability.[41,42] In fact, high formability of Li-strip produced by the cutting was highlighted via the 0T bend test, see Figure 2b.

Materials Characterization: The strips were characterized by 3-D surface topography, measured using optical profilometry (Zygo New View 9000); surface quality, edge cracking and material pull-out by optical

microscopy and scanning electron microscopy (SEM); and hardness (strength) measurement by Vickers indentation.

The surface roughness (S_a and R_a) on the cut surface and back surface of the strip (length x width) was estimated from 3-D surface topography profiles taken at 3 different locations on the surface. Sa was the area-based arithmetic average roughness based on the whole areal profile, as was typical, ignoring the lay of the surface.[48] R_a was the arithmetic average roughness obtained from 2-D line scans all made across the profile lay, as was the norm.[49] For obtaining the R_a, line scans were made at 5 different locations in the areal profile. Similar roughness characterization was also done with a commercial Li foil, removed from an AA 1.5 V Li battery. Based on the measurements, the attributes of the HCE and FC strips were benchmarked against those of the commercial Li battery foil.

Quantitative analysis of the optical surface topography profiles, as well as SEM observations, revealed that the lay on the two surfaces of the strip produced by the cutting had different orientations. On the cut surface, the lay was parallel to the strip length direction while on the back surface the lay was mainly in the direction of the strip width. The back surface lay was a well-known consequence of the nature of the shear deformation in the shear zone AB (Figure 1), which causes periodic microscopic "grooves" to be formed parallel to the strip width.[24]

The strength of the Li strips and of the initial workpiece ingot was estimated by Vickers micro-indentation at 100 gm load. This strength is reported in Table 1 and elsewhere, both in terms of the hardness (HV), and as a yield strength (σ_y = HV/3).[39]

Process Energy Analysis – Benchmarking Against Conventional Extrusion/Rolling: It was of interest to compare the process energy for Li strip production by the cutting-based methods with that of conventional deformation processing by multistage rolling and/or extrusion. This was done using the process specific energy (energy/volume or energy/mass) as the parametric attribute. The specific energy for Li strip production was estimated by cutting from force and material removal rate measurements (Figure 6). The specific energy for the cutting was the power ($F_c V_o$) divided by the material removal rate (mass or volume of Li strip produced per second). The volumetric removal rate was $V_o \times t_0 \times$ strip width, which was also directly measured.

The corresponding specific energy, for production of Li strip by current forming methods (extrusion/rolling), was difficult to estimate or predict, due to lack of published data for process power, as well as details about industrial processing schedules. In view of this, the following was done. A specific energy comparison was carried out for production of Al and 316ss, for which industrial rolling schedules were available.[13–15] For these materials, the corresponding specific energy estimates for strip production was also obtained by the HCE/FC from force measurement. A lower-bound estimate of the specific energy for Li strip production was next made by extrusion/rolling, using process parameter data from patents.[8,19] These two sets of data – viz, 1) the energy for Al and 316ss strip, and 2) predicted extrusion/rolling specific energy for Li strip – were then used to assess the process energy benefits, if any, of the cutting-based processes vis-à-vis conventional deformation processing (i.e., rolling and extrusion).

For the first (broader) energy comparison, rolling schedules typical of industrial sheet processing of 316ss, and an Al alloy similar to Al 6061 were used. The schedule used was reduction from initial block thickness of 700 mm to final sheet thickness of 0.5 mm, involving nominally 23 hot rolling passes (to 3.5 mm thickness), followed by 2 cold rolling passes to final 0.5 mm thickness. The hot/cold rolling temperatures were nominally 575 °C/25 °C for the Al alloy; and 1200 °C/25 °C for the 316ss. Details about the deformation modeling, process conditions and material properties are found in Ref. [14]. The energy was estimated as the sum of the workpiece pre-heating energy (only in hot rolling) and deformation processing energy (hot/cold rolling via simulation) for the multistage rolling process.

For the second calculation, viz., the lower-bound estimate of specific energy for Li foil (500 µm thickness) processing by combined extrusion/rolling, the following process schedule was used and obtained from Li process patents[8,19] – Stage 1: extrusion of 2.5 mm thickness strip from a 200 mm diameter billet (length 300 mm), followed by, Stage 2: plane-strain rolling of the 2.5 mm strip to final thickness of 500 µm (0.5 mm). The lithium flow stress was taken as $\sigma_y = 2$ MPa, the quasi-static value obtained from Vickers indentation. The frictional condition at the extrusion die – Li workpiece interface was assumed to be sticking friction, with constant interface (friction) shear stress (k) of 1 MPa ($k = \sigma_y/2$). The energy calculation details were then as follows, based on well-accepted deformation processing models for extrusion and rolling.[11]

Extrusion Stage: The specific energy (energy/volume) for the extrusion stage was obtained as sum of the energy purely associated with the deformation shape change (p_d) and the frictional energy dissipation (p_f).

$$p_d = \sigma_y \ (1.06 + 1.55 \ ln \ R) \tag{3}$$

where $R = A_0/A$ is the extrusion ratio (A_0 and A represent the initial and final ingot cross sectional areas respectively). This expression is based on Refs. [11].

For our Li case of a 200 mm diameter ingot being reduced to a final strip of thickness 2.5 mm, the extrusion ratio could be approximated as $R = 200/2.5 = 80$. Equation (3) then gives the shape-change specific energy as p_d = 15.7 MPa (≈0.016 J mm^{-3}). The specific energy (p_f) associated with the frictional dissipation is given by[11]

$$p_f = \frac{4kL}{D_0} \tag{4}$$

where L is the length of the billet at the inlet of the extrusion die, and D_o is the inside diameter of the extrusion die at inlet (= billet diameter). For our case, L and D_o are 200 and 300 mm respectively. p_f is then obtained as 6 MPa (0.006 J mm^{-3}). The total extrusion specific energy is then $p_e = p_d + p_f$ = 21.7 MPa (≈0.022 J mm^{-3}).

Rolling Stage: A lower bound for the rolling specific energy (p_r) was obtained by modeling the rolling reduction as plane-strain compression, with fixed contact length between die and workpiece[11]

$$p_r = \left[1.15 \ \sigma_y ln \left(\frac{h_i}{h_f}\right)\right] \times \frac{1}{\eta} \tag{5}$$

where h_i and h_f are the thickness of the workpiece material at the inlet and exit of the roll, respectively; and $\eta = 0.5$ is a typical process efficiency factor that accounts for friction and redundant deformation.[11] For the Li rolling schedule, h_i = 2.5 mm, and h_f = 0.5 mm (final strip thickness). p_r = 7.4 MPa (≈0.0074 J mm^{-3}) is then obtained. The total process specific energy for the combined extrusion/rolling of Li strip is then obtained as $p_e + p_r$ = 29.1 MPa (≈0.029 J mm^{-3}).

Supporting Information

Supporting Information is available from the Wiley Online Library or from the author.

Acknowledgements

D.P.M. and J.B.M. contributed equally to this work. This research was supported in part by NSF grants CMMI 2100568, DMR 2104745, and PFI 2141180 to Purdue, the Laboratory Directed Research & Development (LDRD) program at Sandia National Laboratories, and DOE STTR award DE-SC0023894 to M4 Sciences. The authors would like to acknowledge contributions by Brynal A. Benally and Benjamin W. Juba from Sandia National Laboratories for Li compositional analysis. Sandia National Laboratories is a multi-mission laboratory managed and operated by National Technology and Engineering Solutions of Sandia LLC, a wholly owned subsidiary of Honeywell International Inc. for the U.S. Department of Energy's National Nuclear Security Administration under contract DE-NA0003525. This paper describes

objective technical results and analysis. Any subjective views or opinions that might be expressed in the paper do not necessarily represent the views of the U.S. Department of Energy or the United States Government.

Conflict of Interest

The authors declare no conflict of interest.

Data Availability Statement

The data that support the findings of this study are available from the corresponding author upon reasonable request.

Keywords

anodes, cutting, foil, Lithium batteries

Received: August 8, 2023
Revised: December 12, 2023
Published online:

[1] P. Hovington, M. Lagacé, A. Guerfi, P. Bouchard, A. Mauger, C. M. Julien, M. Armand, K. Zaghib, *Nano Lett.* **2015**, *15*, 2671.
[2] G. Harper, R. Sommerville, E. Kendrick, L. Driscoll, P. Slater, R. Stolkin, A. Walton, P. Christensen, O. Heidrich, S. Lambert, A. Abbott, K. Ryder, L. Gaines, P. Anderson, *Nature* **2019**, *575*, 75.
[3] C. Niu, D. Liu, J. A. Lochala, C. S. Anderson, X. Cao, M. E. Gross, W. Xu, J.-G. Zhang, M. S. Whittingham, J. Xiao, J. Liu, *Nat. Energy* **2021**, *6*, 723.
[4] R. Schmuch, R. Wagner, G. Hörpel, T. Placke, M. Winter, *Nat. Energy* **2018**, *3*, 267.
[5] M. Wan, S. Kang, L. Wang, H.-W. Lee, G. W. Zheng, Y. Cui, Y. Sun, *Nat. Commun.* **2020**, *11*, 829.
[6] W. Wu, W. Luo, Y. Huang, *Chem. Soc. Rev.* **2023**, *52*, 2553.
[7] B. Acebedo, M. C. Morant-Miñana, E. Gonzalo, I. Ruiz De Larramendi, A. Villaverde, J. Rikarte, L. Fallarino, *Adv. Energy Mater.* **2023**, *13*, 2203744.
[8] B. K. Hovsepian, Rolling of lithium., United States patent 3,721,113. **1972**.
[9] E. O. Jonsson, F. Larsson, *Securing Lithium Foil Supply in a Future Imbalanced Market, Master of Science Thesis*, Chalmers University of Technology, Goteborg, Sweden **2016**.
[10] W. A. Backofen, *Metall. Trans.* **1973**, *4*, 2679.
[11] G. E. Dieter, *Mechanical Metallurgy*, 3rd ed., McGraw-Hill, New York **1986**;
[12] *ASM Handbook, Metalworking: Bulk Forming, 14A*, ASM International, Materials Park, OH, USA **2005**.
[13] V. Burt, *Aluminum Science and Technology*, *2A*, ASM International, Materials Park, OH, USA **2018**.
[14] S. Chandrasekar, K. P. Trumble, J. B. Mann, A. Rohatgi, M. Efe, *US OSTI Report*, **2022**, *1900616*.
[15] R. J. Fruehan, O. Fortini, H. W. Paxton, R. Brindle,*US OSTI Report*, **2000**, *769470*.
[16] J. B. Mann, D. P. Mohanty, A. B. Kustas, B. S. P. Rodriguez, M. N. Issahaq, A. Udupa, T. Sugihara, K. P. Trumble, R. M'saoubi, S. Chandrasekar, *CIRP Ann.* **2023**, *72*, 45.
[17] Y. Sakamoto, Y. Tonooka, Y. Yanagisawa, *Energy Convers. Manage.* **1999**, *40*, 1129.
[18] F. S. Froes, M. N. Gungor, M. Ashraf Imam, *J. Met.* **2007**, *59*, 28.
[19] R. Laliberte, J. Dube, Process and apparatus for manufacturing lithium of lithium alloy thin sheets for electrochemical cells. United States patent 7, **2007**, *194*, 884.
[20] T. Sedlatschek, J. Lian, W. Li, M. Jiang, T. Wierzbicki, M. Z. Bazant, J. Zhu, *Acta Mater.* **2021**, *208*, 116730.
[21] C. D. Fincher, D. Ojeda, Y. Zhang, G. M. Pharr, M. Pharr, *Acta Mater.* **2020**, *186*, 215.
[22] A. Masias, N. Felten, R. Garcia-Mendez, J. Wolfenstine, J. Sakamoto, *J. Mater. Sci.* **2019**, *54*, 2585.
[23] N. K. Sundaram, Y. Guo, S. Chandrasekar, *Phys. Rev. Lett.* **2012**, *109*, 106001.
[24] J. T. Black, *ASME J. Eng. Ind.* **1972**, *94*, 307.
[25] H. Yeung, K. Viswanathan, W. D. Compton, S. Chandrasekar, *Proc. Natl. Acad. Sci. USA* **2015**, *112*, 9828.
[26] M. C. Shaw, *Metal cutting principles*, Oxford University Press, United Kingdom **1984**.
[27] T. L. Brown, C. Saldana, T. G. Murthy, J. B. Mann, Y. Guo, L. F. Allard, A. H. King, W. D. Compton, K. P. Trumble, S. Chandrasekar, *Acta Mater.* **2009**, *57*, 5491.
[28] A. Kobayashi, *Machining of Plastics*, 1st ed., McGraw-Hill, New York, **1967**.
[29] K. Kendall, *Molecular adhesion and its applications: the sticky universe.*, Springer, United States **2001**.
[30] A. Udupa, K. Viswanathan, S. Chandrasekar, *Europhys. Lett.* **2020**, *129*, 46001.
[31] W. Moscoso, M. R. Shankar, J. B. Mann, W. D. Compton, S. Chandrasekar, *J. Mater. Res.* **2007**, *22*, 201.
[32] T. Sugihara, A. Udupa, K. Viswanathan, J. M. Davis, S. Chandrasekar, *Sci. Adv.* **2020**, *6*, eabc8900.
[33] J. A. Schey, *J. Appl. Metalwork.* **1980**, *1*, 48.
[34] G. E. Dieter, H. A. Kuhn, S. L. Semiatin, *Handbook of Workability and Process Design*, ASM International, Materials Park, OH, USA **2003**.
[35] H. Yeung, K. Viswanathan, W. D. Compton, S. Chandrasekar, *Proc. Natl. Acad. Sci. USA* **2015**, *112*, 9828.
[36] *ASM Metals Handbook Volume 2*, ASM International, Materials Park, OH, USA **1981**.
[37] H. R. Le, M. P. F. Sutcliffe, *Wear* **2000**, *244*, 71.
[38] J. Becking, A. Gröbmeyer, M. Kolek, U. Rodehorst, S. Schulze, M. Winter, P. Bieker, M. C. Stan, *Adv. Mater. Interfaces* **2017**, *4*, 1700166.
[39] D. Tabor, *Rev. Phys. Technol.* **1970**, *1*, 145.
[40] S. L. Sass, *Appl. Phys. Lett.* **1969**, *14*, 365.
[41] D. Sagapuram, M. Efe, W. Moscoso, S. Chandrasekar, K. P. Trumble, *Acta Mater.* **2013**, *61*, 6843.
[42] A. B. Kustas, D. Sagapuram, K. P. Trumble, S. Chandrasekar, *Metall. Mater. Trans. A* **2016**, *47*, 3095.
[43] A. Masias, N. Felten, R. Garcia-Mendez, J. Wolfenstine, J. Sakamoto, *J. Mater. Sci.* **2019**, *54*, 2585.
[44] C. D. Fincher, D. Ojeda, Y. Zhang, G. M. Pharr, M. Pharr, *Acta Mater.* **2020**, *186*, 215.
[45] T. Sedlatschek, J. Lian, W. Li, M. Jiang, T. Wierzbicki, M. Z. Bazant, J. Zhu, *Acta Mater.* **2021**, *208*, 116730.
[46] F. S. Froes, M. N. Gungor, M. Ashraf Imam, *J. Met.* **2007**, *59*, 28.
[47] T. L. Brown, C. Saldana, T. G. Murthy, J. B. Mann, Y. Guo, L. F. Allard, A. H. King, W. D. Compton, K. P. Trumble, S. Chandrasekar, *Acta Mater.* **2009**, *57*, 5491.
[48] X. Jiang, P. J. Scott, D. J. Whitehouse, L. Blunt, *Proc. R. Soc. A* **2007**, *463*, 2071.
[49] H. Dagnall, *Exploring Surface Texture*, Rank Taylor Hobson, Leicester, UK **1980**.